PHYSICAL REVIEW B **72**, 214403 (2005)

Antiferromagnetic dipolar ordering in $[\mathrm{Co_2MnGe/V}]_N$ multilayers

A. Bergmann,[1,*] J. Grabis,[1] B. P. Toperverg,[1,2,†] V. Leiner,[1,3] M. Wolff,[1,3] H. Zabel,[1] and K. Westerholt[1]
[1]*Department of Physics, Ruhr-University Bochum, D-44780 Bochum, Germany*
[2]*Petersburg Nuclear Physics Institute, Gatchina, 188300 St. Petersburg, Russia*
[3]*Institute Laue Langevin, BP 156, F-38042, Grenoble Cedex 9, France*

(Received 25 January 2005; revised manuscript received 5 August 2005; published 2 December 2005)

We have studied $[\mathrm{Co_2MnGe/V}]_N$ multilayers with a thickness of the V layers t_V between 1.5 and 10 nm and a fixed thickness of the Heusler layer $t_{\mathrm{Co_2MnGe}}=3$ nm by x-ray scattering, neutron reflectivity, and magnetization measurements. In the thickness range $t_\mathrm{V}\leqslant 3$ nm neutron reflectivity results provide clear evidence for an antiferromagnetic (af) interlayer long-range order below a Néel temperature T_N. The interlayer long range order does not show an oscillating character and is stabilized by a weak af coupling field $H_\mathrm{af}\approx 100$ Oe. We attribute the af coupling to magnetic dipolar stray fields originating from magnetically rough surfaces of a granular $\mathrm{Co_2MnGe}$ microstructure. In the thickness range $t_\mathrm{V}\geqslant 4$ nm the multilayers undergo a cluster glass transition at $T_\mathrm{f}\approx 150$ K. At high temperatures above T_N or T_f the mutilayers are superparamagnetic with a huge cluster magnetic moment $\mu_\mathrm{c}\geqslant 10^5\mu_\mathrm{B}$.

DOI: 10.1103/PhysRevB.72.214403 PACS number(s): 75.50.Cc, 75.50.Ee, 75.70.−i, 81.15.Cd

I. INTRODUCTION

In recent years an upsurge of interest has been noticed in ferromagnetic metals with 100% spin polarization at the Fermi level due to their potential in the rapidly evolving field of spintronics.[1–3] Electronic energy band structure calculations revealed the possible existence of several fully spin polarized Heusler compounds, among them PtMnSb, NiMnSb,[4] $\mathrm{Co_2MnGe}$, $\mathrm{Co_2MnSi}$,[5] and $\mathrm{Co_2Cr_{0.6}Fe_{0.4}Al}$.[6] The Heusler compounds $\mathrm{Co_2MnSi}$ and $\mathrm{Co_2MnGe}$ combine a high ferromagnetic Curie temperature (960 K and 900 K, respectively) and a high volume magnetization. Therefore, they are, in principle, ideal materials for applications in spinelectronics, such as spin injection into semiconductors, tunneling magnetoresistance (TMR),[7] and giant magnetoresistance (GMR)[8] elements. However, experimentally the realization of full spin polarization in thin films of the Heusler compounds is a difficult task. Until now the degree of spin polarization measured experimentally is always definitely less than 100%.[9–11] The reason for this reduction is usually associated with site disorder in the ordered ternary Heusler compounds, since only the perfectly ordered alloy (space group $L2_1$) develops a gap in the minority spin band.[5,12] Interfaces in thin film heterostructures combining the Heusler alloys with other materials are of utmost importance for spintronic devices. However, these compounds are prone to interdiffusion and site disorder, which both have the tendency to suppress the full spin polarization.[5,12]

We have started systematic investigations of metallic multilayers of the Heusler phase $\mathrm{Co_2MnGe}$ with other metals like V, Au, and Cr.[13] The aim of this research is twofold. On the one hand, high quality multilayers or superlattices are ideally suited to study the structural quality of interfaces by x-ray or neutron reflectivity methods. On the other hand, we were interested in the basic question whether an oscillatory interlayer exchange interaction (IEC), which exists in most magnetic/nonmagnetic multilayer systems of the transition metals,[14] can also be observed in $\mathrm{Co_2MnGe}$-based multilayers. In the case of a positive answer one could, e.g., prepare antiferromagnetically coupled multilayers with a presumably large GMR effect.

In fact, of the many different multilayer systems we have studied up to now,[13] we found only in the $[\mathrm{Co_2MnGe/V}]$ system first indications from magnetization measurements that an antiferromagnetic interlayer coupling might exist. This was confirmed later by preliminary neutron reflectivity measurements.[15] In the present paper we will report on a detailed investigation of the magnetic ordering phenomenon in $[\mathrm{Co_2MnGe/V}]$ multilayers with variable V thickness. It will turn out that the interlayer magnetic ordering is unconventional and definitely different from the IEC mechanism. The magnetic order is directly related to the peculiarities of the magnetism in very thin Heusler layers.

This paper is organized as follows: In Sec. II we describe the sample preparation and introduce the experimental methods applied. Section III contains a characterization of the multilayer structure using specular and off-specular x-ray scattering measurements. In Sec. IV we report on the magnetic properties with special emphasis on a quantitative interpretation of off-specular magnetic neutron scattering and derive a magnetic phase diagram. In Sec. V we discuss the microscopic origin of the magnetic ordering phenomenon in $[\mathrm{Co_2MnGe/V}]_n$ multilayers, Sec. VI provides conclusions and a summary.

II. SAMPLE PREPARATION AND EXPERIMENTAL

The samples used in this study were grown by dual source radio frequency (rf)-sputtering at a pressure of 5×10^{-3} mbar Ar and a substrate temperature of 300 °C on $\mathrm{Al_2O_3}$ *a*-plane, as described in detail elsewhere.[13] We prepared a series of multilayers with a constant nominal thickness of the $\mathrm{Co_2MnGe}$ layers $t_{\mathrm{Co_2MnGe}}=3.0$ nm and variable V interlayer thicknesses $t_\mathrm{V}=1.5$, 2.0, 2.5, 3.0, 4.0, 5.0, and 10.0 nm. The number of bilayers was 20 for $t_\mathrm{V}=1.5$, 4.0, and 10.0 nm and 50 for the other multilayers. In Table I the growth parameters of the samples are listed. One should note

TABLE I. Overview of the structural parameters for the $[\mathrm{Co_2MnGe}(t_{\mathrm{Co_2MnGe}})/\mathrm{V}(t_{\mathrm{V}})]_N$ multilayers with the nominal thickness (first row), the number of periods N (second row), the experimental thickness (third row), and the total rms roughness parameters derived from the x-ray reflectivity data (see main text).

Nominal thickness			Experimental thickness		rms roughness	
t_{V} (nm)	$t_{\mathrm{Co_2MnGe}}$ (nm)	N	t_{V} (nm)	$t_{\mathrm{Co_2MnGe}}$ (nm)	σ_{V} (nm)	$\sigma_{\mathrm{Co_2MnGe}}$ (nm)
1.5	3	20	1.45	2.9	0.4	0.4
2	3	50	2.35	3.0	0.5	0.65
2.5	3	50	3.0	3.0	0.75	0.55
3	3 (#1)	50	3.4	3.4	0.65	0.85
3	3 (#2)	50	2.8	2.9	0.85	0.9
4	3	20	3.8	3.0	0.9	0.75
5	3	50	5.0	2.9	0.95	0.7

that for $t_{\mathrm{V}}=3$ nm we have prepared two samples with slightly different preparation conditions. The samples are referred to as #1 and #2 in the figures below.

The magnetic measurements of the samples were carried out by a commercial SQUID-magnetometer (Quantum Design MPMS system). The chemical structure of the multilayers was characterized by x-ray scattering at the beamline W1 at the HASYLAB (Hamburg, Germany) using a diffractometer with a standard two circle setup. The photon energy was chosen to be $h\nu=8048$ eV, corresponding to Cu $K\alpha$ radiation ($\lambda=0.154$ nm) or $h\nu=7000$ eV ($\lambda=0.177$ nm), which yields a slightly better contrast of the scattering lengths.

We have studied specular and diffuse (off-specular) scattering in the small angle regime combining longitudinal Q_z, offset Q_z, and transverse Q_x scan geometries (see Fig. 1).[16] The specular intensity was collected using standard θ-2θ scans along Q_z (with z as growth direction). A structurally well-defined multilayer periodicity gives rise to Bragg peaks at $Q_z=2\pi n/\Lambda$, where Λ is the bilayer thickness and n is an integer. Interdiffusion at the interfaces leads to diffuse intensity, which is not localized along the Q_z direction, but spreads out in the reciprocal space. To map out diffuse scattering, offset Q_z and Q_x scans were taken. The offset Q_z scan corresponds to the longitudinal Q_z scan, but with the sample rotated by $\Delta\theta$ from the specular direction, such that only diffuse intensity is collected (see Fig. 1). If the interface roughness of the multilayers is correlated along the growth direction, the features of the specular scan will be replicated. Transverse Q_x scans at the Q_z position of the multilayer Bragg peak give information on the *in-plane* correlation length and correlated roughness.[17,18] If the probed Q_x regime is large enough, it is possible to distinguish between short-range disorder, resulting from roughness and long-range disorder e.g., from terracing. Experimentally these scans are often realized by rocking scans, i.e., fixing the scattering angle 2θ and varying α_i and α_f so that $\alpha_i+\alpha_f=$const. If Q_x/Q_z is small, these scans approximate Q_x scans in reciprocal space. With the help of appropriate software it is also possible to perform proper Q_x scans, which we preferred for our measurements.

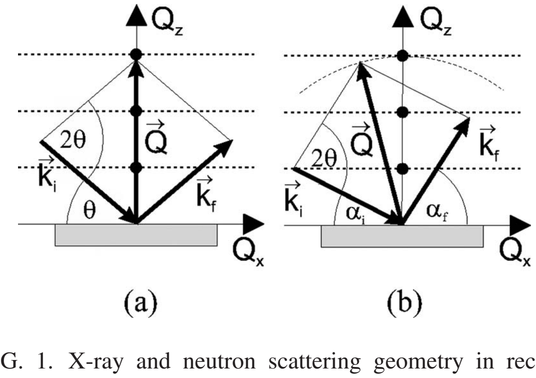

(a) (b)

FIG. 1. X-ray and neutron scattering geometry in reciprocal space for (a) a specular reflectivity ($\theta-2\theta$ scan, $Q_x=0$) and (b) diffuse scattering (Q_x scan, Q_z constant). Bragg peaks in the specular reflectivity and diffuse Bragg sheets are schematically shown as dots and dotted lines, respectively.

In order to obtain information on the in- and out-of-plane crystalline structure, high-angle out-of-plane Bragg scans and grazing incidence in-plane Bragg scans using Cu $K\alpha$ radiation were carried out.

Unpolarized and polarized neutron reflectivity (PNR) measurements were performed to identify and characterize the magnetic structure of the multilayers. We obtained these data at the Institute Laue-Langevin in Grenoble (France) mainly with the ADAM reflectometer,[19] but also with the EVA instrument.[20] The reflectometer ADAM is an angle dispersive fixed wavelength machine working at $\lambda=0.44$ nm. Transmission supermirrors allow the polarization and analysis of the neutron spin direction. Using 180° spin flippers it is possible to measure the non-spin-flip (NSF) $[(++)$ and $(--)]$ and spin-flip (SF) $[(+-)$ and $(-+)]$ scattered intensities, which are collected by a 2D position sensitive detector. The efficiency of spin-polarizing and analyzing devices is typically 97%. A displex cryostat and a solenoid serve for a temperature range from 10 to 600 K and a field range up to 1 T. We used the ADAM reflectometer for polarized and unpolarized reflectivity studies applying the same scan geometries as in the x-ray experiments (see Fig. 1).

In the polarized neutron reflectivity scans all four cross sections $(++)$, $(--)$, $(+-)$, and $(-+)$ are measured. Here $+(-)$ designates the up (down) spin polarization of the incident and reflected neutrons relative to an applied field at the sample position defining a polarization vector $\mathbf{P}$, here paral-

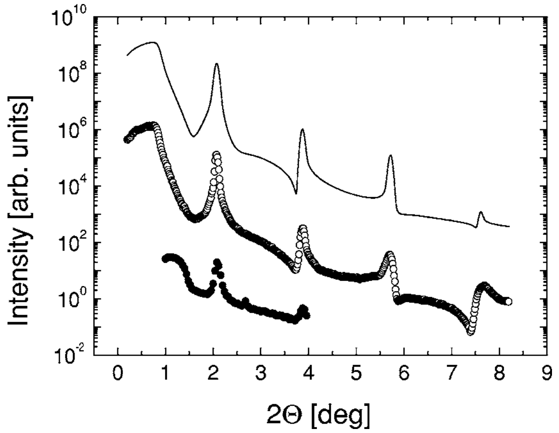

FIG. 2. X-ray reflectivity scan of a $[\mathrm{Co_2MnGe(3\ nm)/V(2\ nm)}]_{50}$ multilayer measured at $h\nu=7000$ eV. The open symbols denote the measured intensity. The simulation is shown by the full line, which is offset by a constant factor from the experimental data for clarity reasons. The filled circles (bottom curve) show the corresponding off-specular scan ($\theta-0.3°$).

lel to the sample plane. The non-spin-flip intensities contain information on the chemical structure and are sensitive to the projection of the in-plane magnetization of the sample parallel to **P**. This leads to a splitting of the $(++)$ and $(--)$ intensities, if the sample is ferromagnetic. The spin-flip channels are sensitive to the magnetic induction projected perpendicular to **P**. The spin flip is of pure magnetic origin and does not occur in coherent nuclear scattering. By measuring SF and NSF reflectivities the magnitude and orientation of the in-plane magnetic induction $B=4\pi M$ of the sample can be determined.

III. STRUCTURAL CHARACTERIZATION

In Fig. 2 we show the small angle x-ray reflectivity scan and the corresponding off-specular ($\theta-0.3°$) scan of a $[\mathrm{Co_2MnGe(3\ nm)/V(2\ nm)}]_{50}$ sample with a nominal thickness (as calculated from the sputtering rates) of 3 nm for $\mathrm{Co_2MnGe}$ and 2 nm for V. The data were taken at $h\nu=7000$ eV. Specular and off-specular data are scaled to the same intensity, allowing a direct comparison. Above the critical angle for total reflection θ_c the superstructure gives rise to Bragg peaks superimposed on the Fresnel reflectivity. We observe sharp superlattice reflections up to fourth order, revealing good interface quality and low fluctuations of the layer thickness. The off-specular data mainly replicate the specular one, indicating a significant correlated roughness along the growth direction. The simulation using the Parratt formalism[21] (see Fig. 2) reproduces the thickness of the layers as well as their total rms roughness. (We refer to the roughness as *total*, because it contains correlated and uncorrelated parts, which cannot be distinguished by Q_z scans.) In good agreement with the nominal thickness we get $t_{\mathrm{V}}=2.35$ nm and $t_{\mathrm{Co_2MnGe}}=3.0$ nm. The interface roughness is $\sigma_{\mathrm{V}}=0.5$ nm and $\sigma_{\mathrm{Co_2MnGe}}=0.65$ nm. These values are generated by the Parratt formalism from the spatial profile of the scattering length density; the interfacial roughness is included by varying the density with an error function. For the $[\mathrm{Co_2MnGe/V}]$ multilayers we find that the scattering length densities in the V layers as well as in the $\mathrm{Co_2MnGe}$ layers deviate slightly from their bulk value.

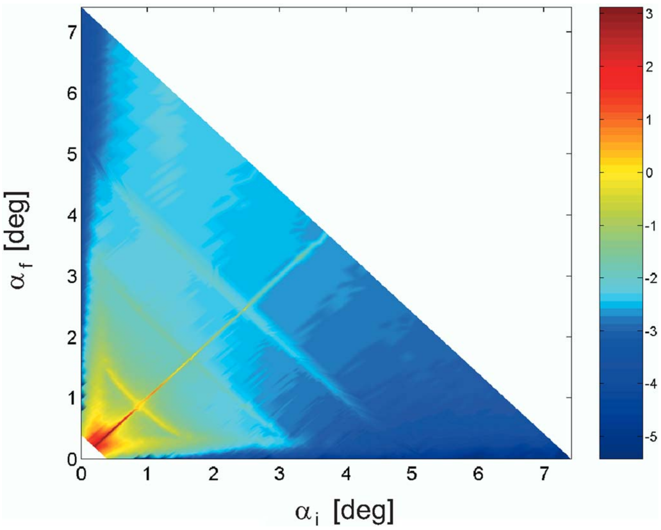

FIG. 3. (Color online) Two-dimensional (2D) map of the x-ray intensity scattered from the $[\mathrm{Co_2MnGe(3\ nm)/V(2\ nm)}]_{50}$ multilayer as a function of the angle of incidence α_i and scattering α_f, respectively. The logarithmic intensity color scale is shown on the right-hand side.

Additional information on the in-plane structure of the interfaces and their correlations can be obtained by analyzing the diffuse scattering. One important parameter which can be derived is the in-plane correlation length ξ.[17,18] In Fig. 3 we show a 2D map with the logarithm of the reflectivity contours plotted as a function of x-ray incident (α_i) and exit angles (α_f). The diagonal ridge at $\alpha_i=\alpha_f$ is the specularly reflected intensity. If the interfacial roughness is perfectly correlated in the vertical direction, the diffuse intensity along Q_z would be peaked at the Bragg conditions, visible as Bragg sheets. For random perpendicular roughness, the diffuse intensity will be spread out uniformly in Q_z.[17,18] The multilayers studied here have a roughness correlation somewhere between these limiting cases. The Bragg sheets can easily be identified. The perpendicular roughness correlation exists, but the intensity is low, indicating that random roughness is predominant.

Figure 4 shows a transverse Q_x scan of the sample $[\mathrm{Co_2MnGe(3\ nm)/V(2\ nm)}]_{50}$ together with a simulation. The Q_x scans of the multilayers are usually taken at the Q_z values corresponding to the second-order Bragg peak. The experimental data are corrected for footprint effects arising from the fact that the probed volume of the sample changes with the angle of incidence. Besides the Yoneda wings, other optical features arising from the multilayer periodicity are visible. For the simulation we used the Mingh model,[22] which describes an intermediate case between uncorrelated and completely correlated roughness and assumes that vertical correlations do not depend on the lateral scale of the roughness. The parameters used for this model are the vertical correlation length L_{v}, the horizontal correlation length L_h,

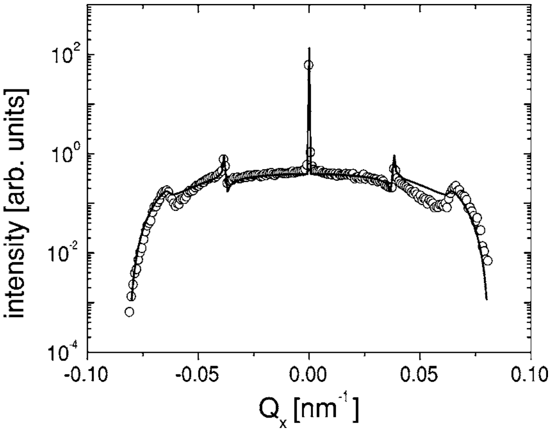

FIG. 4. Transverse Q_x scan of the $[Co_2MnGe(3\ nm)/V(2\ nm)]_{50}$ sample at the position of the second-order Bragg peak at $Q_x=2.4\ nm^{-1}$ (dots) together with a fit within the Mingh model (Ref. 22) (line).

and the "jaggedness" parameter h. The vertical correlation was taken from the out-of-plane coherence length obtained from large angle diffraction (see below). The jaggedness and the in-plane correlation length are left as the only free parameters, h being a value between 0.1 and 1. For small h values the surface is extremely jagged; if $h=1$, the surface has smooth hills and valleys.[18] Best fits could be achieved for $L_h=20$ nm and $h=1$. We attribute the horizontal correlation length to long-range disorder from grain boundaries.

Information on the crystalline structure of the multilayers is obtained by large angle diffraction. In Fig. 5 a longitudinal scan of the sample $[Co_2MnGe(3\ nm)/V(2\ nm)]_{50}$ at $\lambda=0.177$ nm is depicted. The multilayer possesses pure (220) out-of-plane texture for Co_2MnGe as well as for the V layers. Aside from the fundamental Bragg peak, the multilayer exhibits a rich satellite structure caused by chemical modulations. The spacing derived from the position of these satellite peaks corresponds exactly to the chemical modulation as determined from reflectivity measurements. Satellite peaks up to the order $l=+2$ and $l=-3$ can be resolved, indicative for a coherently grown superstructure in the growth direction.

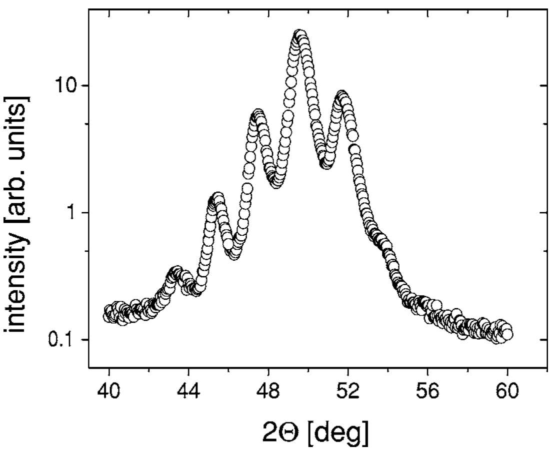

FIG. 5. Out-of-plane x-ray Bragg scan of the $[Co_2MnGe(3\ nm)/V(2\ nm)]_{50}$ multilayer at $\lambda=0.177$ nm.

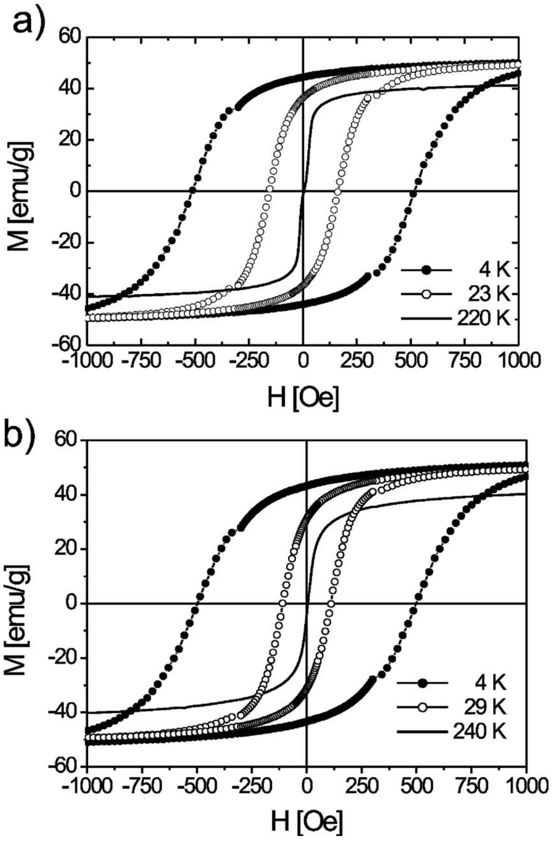

FIG. 6. Hysteresis loops of the multilayers $[Co_2MnGe(3\ nm)/V(3\ nm)]_{50}$ (#1) (a) and $[Co_2MnGe(3\ nm)/V(4\ nm)]_{20}$ (b) measured at different temperatures indicated in the figure. The mass in the magnetization unit refers to the magnetic layer only.

From the width of the satellite peaks at half maximum (FWHM) $\Delta(2\Theta)$ we derive the out-of-plane coherence length of the multilayer D_{coh} using the Scherrer equation $D_{coh}=0.89\lambda/[\Delta(2\Theta)\cdot\cos(\Theta)]$.[23] We estimate $D_{coh}=13$ nm, thus comprising about two superlattice periods. The fundamental Bragg peak in Fig. 5 is positioned at $2\Theta=49.75°$, i.e., at the middle position between the V (110) Bragg peak at $2\Theta=48.8°$ and the Co_2MnGe (220) peak at $2\Theta=51.6°$, as expected for a coherently strained multilayer. As revealed by in-plane rocking scans, all samples exhibit a broad distribution of in-plane Bragg peaks. Thus the samples can be characterized as polycrystalline multilayers rather than superlattices.

IV. MAGNETIC PROPERTIES

In Fig. 6 we depict magnetic hysteresis loops for $[Co_2MnGe/V]$ multilayers with a V thickness $t_V=3$ nm (a) and $t_V=4$ nm (b), which are representative for all other multilayers studied. The ferromagnetic saturation magnetization at 4 K is about 50 emu/g, corresponding to 45% of the expected saturation magnetization, if all Heusler layers would exhibit the full bulk magnetization. The reduction should be attributed to the intermixing at the interfaces giving rise to nonferromagnetic or weakly ferromagnetic interlayers. With the roughness parameter derived from the x-ray scattering

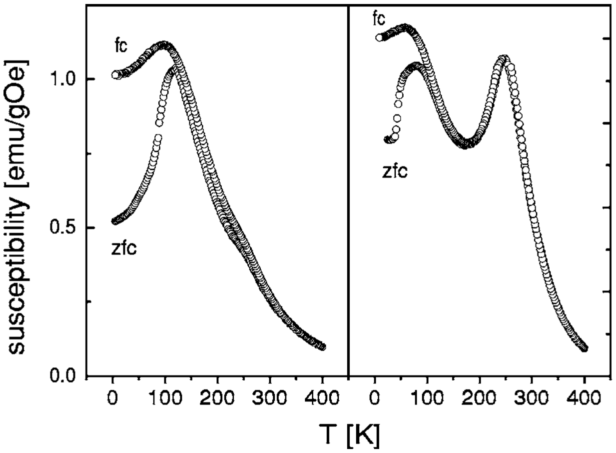

FIG. 7. The dc magnetic susceptibility measured in a field of +10 Oe for the $[Co_2MnGe(3\text{ nm})/V(4\text{ nm})]_{20}$ (left panel) and the $[Co_2MnGe(3\text{ nm})/V(3\text{ nm})]_{50}$ (#1) multilayer (right panel). The field cooled curve (fc) after cooling in $H=+2$ kOe and zero-field cooled curve (zfc) are plotted.

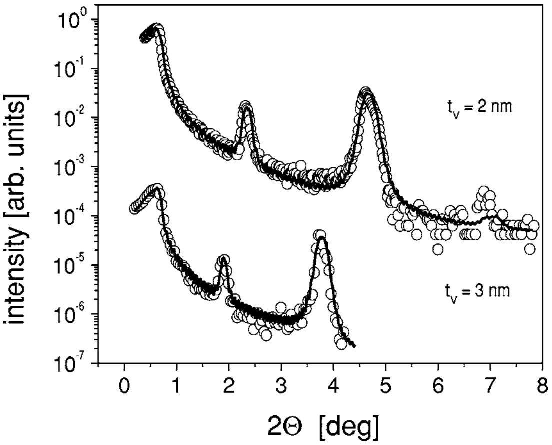

FIG. 8. Specular unpolarized neutron reflectivity scans of the $[Co_2MnGe(3\text{ nm})/V(2\text{ nm})]_{50}$ and the $[Co_2MnGe(3\text{ nm})/V(3\text{ nm})]_{50}$ (#2) multilayers at RT denoted by open symbols. The lines show a fit to the data points by the Parratt formalism. Aside from the structural peaks, half order antiferromagnetic peaks are clearly visible.

data, one can estimate that about 50% of the 3.0 nm thick Co_2MnGe layer belongs to the interfaces.[13] At 4 K the remanent magnetization is 90% of the saturation value, whereas at 220 K the hysteresis loop of the multilayer exhibits a vanishing remanent magnetization, while the saturation magnetization is only slightly reduced. We consider this as a first hint to an antiferromagnetic (af) order. In Fig. 7 we show the susceptibility of the same two samples measured in a dc field of +10 Oe after cooling in zero field (zfc) and in a field of +2000 Oe (fc). For the sample with $t_V=4$ nm the susceptibility is reversible and increases with decreasing temperature down to $T=150$K where one observes the onset of strong magnetic irreversibility and a maximum in $\chi(T)$. This is the classical behavior of a spin glass or cluster glass transition at a freezing temperature T_f.[24] As will be shown below, the susceptibility above T_f reveals the existence of large clusters with ferromagnetic short-range order. Therefore the classification as cluster glass transition seems to be appropriate.

The low-temperature susceptibility of the sample with $t_V=3$ nm shows a strong irreversibility at 100 K. In addition there is a peak in the susceptibility at 250 K, indicating another magnetic phase transition. In the next section we will show that at this transition temperature there is an onset of antiferromagnetic interlayer long-range order.

A. Magnetic neutron scattering

In order to verify the hypothesis of an antiferromagnetic interlayer order in the multilayers we performed specular neutron reflectivity measurements. Figure 8 shows the unpolarized neutron reflectivity scans of the multilayers $[Co_2MnGe(3\text{ nm})/V(2\text{ nm})]_{50}$ and $[Co_2MnGe(3\text{ nm})/V(3\text{ nm})]_{50}$ (#2) measured in zero field at room temperature together with a numerical simulation. In addition to the first-order structural superlattice peak at $2\theta=4.62°$ ($t_V=2$ nm) and $2\theta=3.72°$ ($t_V=3$ nm) there is a magnetic half-order peak at $2\theta=2.32°$ and $2\theta=1.92°$, respectively, due to a doubling of the multilayer periodicity. For the sample $[Co_2MnGe(3\text{ nm})/V(2\text{ nm})]_{50}$ the three half-order af peak can also be resolved. This and the narrow width of the af peaks indicate that the af order might be coherent throughout the whole multilayer stack. We used the structural parameters from the simulation of the x-ray data in Sec. III to simulate the unpolarized neutron reflectivity data in Fig. 8. This reduces the number of free parameters in the fit drastically, so that only the magnetic scattering length densities are left as free parameters. The simulations were performed using the super-iterative routine generalizing a conventional Parratt formalism for the case of reflection of spin 1/2 particles from a stack of magnetic layers.[25,26] At a large number of layers this routine is numerically more stable than the supermatrix formalism proposed earlier.[27,28]

The result of the fit is included in Fig. 8. The magnetic scattering length density for the samples is $Nb_m=0.52\times10^{-6}$ Å^{-2} and $Nb_m=0.4\times10^{-6}$ Å^{-2} for the sample with $t_v=2$ and 3 nm, respectively. This gives a magnetic moment of 1 μ_B and 0.7 μ_B for one Co_2MnGe formula unit, respectively. Note that the fit of unpolarized neutron reflectivity provides values for the sublattice magnetic moments that are too low compared to the saturation values determined with SQUID measurements.

The other samples under study likewise showed an af peak, indicating antiferromagnetic long-range order for a V layer thickness in the range between 1.5 nm$\leqslant t_V \leqslant$3 nm. For the samples with a V layer thickness $t_V \geqslant 4$ nm no af peak could be detected, although the magnetization measurements at higher temperatures showed zero remanence. No indications of an oscillatory character of the af order, as expected for the IEC mechanism, could be discerned.

More detailed insight into the magnetization *vector* arrangement over the mutilayers stack can be achieved by an analysis of PNR data. Figure 9 shows specular PNR data collected for the $[Co_2MnGe(3\text{ nm})/V(2\text{ nm})]_{50}$ (a) and for $[Co_2MnGe(3\text{ nm})/V(3\text{ nm})]_{50}$ (b) multilayer. Two NSF cross sections and the spin-flip $(-+)$ channel are plotted

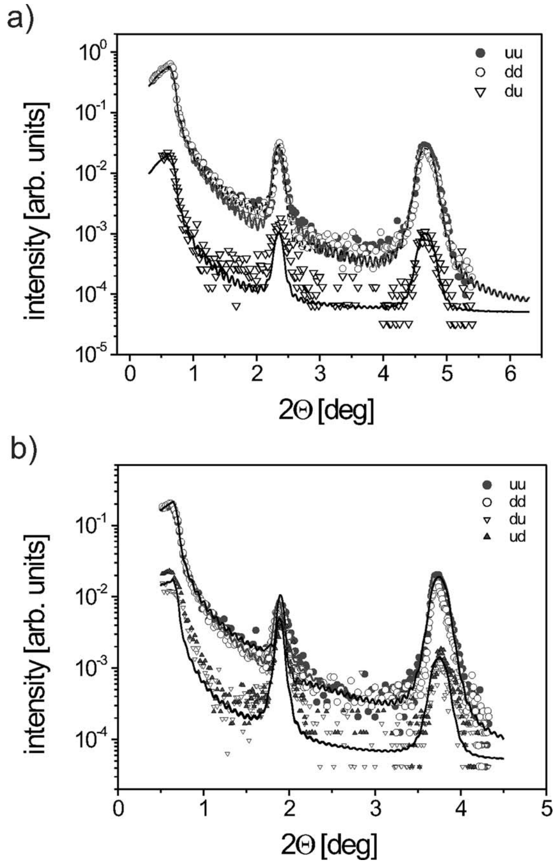

FIG. 9. Specular polarized neutron reflectivity scans for non spin flip ((++) and (−−)) and for spin flip ((−+),(+−)) channels of the multilayers (a) $[\mathrm{Co_2MnGe(3\ nm)/V(2\ nm)}]_{50}$ and (b) $[\mathrm{Co_2MnGe(3\ nm)/V(3\ nm)}]_{50}$ (#1). Measurements taken at 12 K.

together with the result of a computer simulation. The reflectivity scans were performed at 12 K after zero-field cooling and applying a small field of 10 Oe to provide a neutron guide field.

For the multilayer with $t_V=3$ nm there is only a small splitting of the NSF cross sections at the structural first-order peak, well within the range of the error bars. Moreover, the total reflection edges for the (++) and (−−) channel coincide. This indicates that there is essentially no ferromagnetic contribution to the first-order peak in the magnetic ground state. The SF cross section is peaked at the af half-order peak and possesses nearly the same intensity as the NSF cross sections. The specular PNR data can well be simulated using a model, which assumes a coherent af coupling through the multilayer stack, the antiferromagnetic sublattice having the magnetic moments m_1 and $-m_2$, respectively. In order to provide both spin-flip and non-spin-flip reflections at the af peak position, the model assumes that the sublattice magnetizations have projections parallel and perpendicular to the applied field. This is introduced by the fitting parameters $\langle\cos\gamma\rangle$, where γ is the angle between the af axis and the applied field. The transverse dispersion $\langle\sin^2\gamma\rangle$ with the constraint $\langle\cos\gamma\rangle^2\leqslant\langle\cos^2\gamma\rangle=1-\langle\sin^2\gamma\rangle$ accounts for a possible spread in the af axis directions over the sample surface.

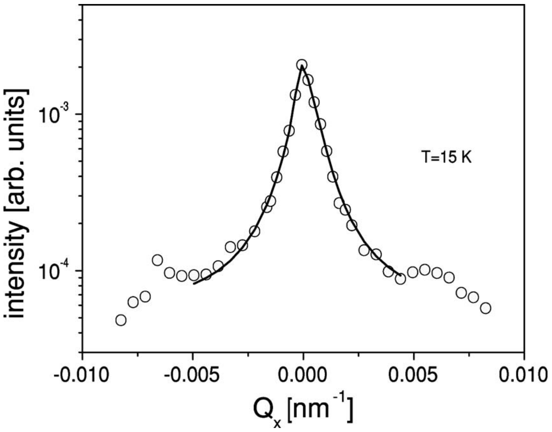

FIG. 10. Neutron transverse scans of the $[\mathrm{Co_2MnGe(3\ nm)/V(3\ nm)}]_{50}$ (#1) sample at the position of the half-order Bragg peak (dots) together with a fit within the framework of the Born approximation (line).

This model can perfectly describe both sets of data in Fig. 9 with the parameters consistent with those obtained from the fit of the data in Fig. 8. In particular, for the sample with $t_V=3$ nm, one gets $m_1=m_2\approx0.8\ \mu_B$/formula unit, $\langle\cos\gamma\rangle=0.7\langle\sin^2\gamma\rangle=0.35$. Then one can speculate on the reasons for an appreciable loss of the layer magnetization in this sample with respect to the saturation magnetization which is $m_1=m_2=2.5\ \mu_B$/formula unit, as well as with respect to the value determined above with magnetometry.

However, the results of our PNR simulations are based on the hypothesis that the layers are homogeneously magnetized over the neutron coherence area: specular reflectivity does not provide any direct information on the lateral length scales of the film, completely ignoring their crystalline structure and possible large-scale inhomogenities. Figure 10 shows a transverse scan of the $[\mathrm{Co_2MnGe(3\ nm)/V(3\ nm)}]_{50}$ (#1) multilayer measured in zero field at 15 K at the position of the af peak. The presence of magnetic off-specular scattering indicates that the magnetization in the single layers is broken up into domains, the size of which being smaller than the longitudinal projection $L_\parallel\sim L/\sin\alpha$ of the neutron coherence length $L\approx1/\Delta Q$, where ΔQ is the uncertainty in the wave vector value due to experimental resolution. The longitudinal projection of the lateral coherence length is estimated to be about 60 μm, while the transverse coherence length (perpendicular to the reflection plane), $L_\perp\sim L$, is only a few nm due to the focusing condition of the monochromator. Remarkable is the fact that in the transverse scan through the af peak no resolution-limited Gaussian profile is apparent, and, in contrast to the structural Bragg peak, the af scan can well be fitted by a Lorentzian line shape. This gives a strong hint that the af peak on the specular reflectivity line is mainly due to a contribution of off-specular scattering to the specular reflection within the range of their overlap. Hence, being simulated with the model given above and assuming only specular reflectivity leads to a false result for this sample.

Therefore quantitative evaluation of both, PNR and off-specular scattering, collected over a broad range of incidence and scattering angles is required for a realistic description of the present system. Figure 11 depicts an unpolarized 2D α_i

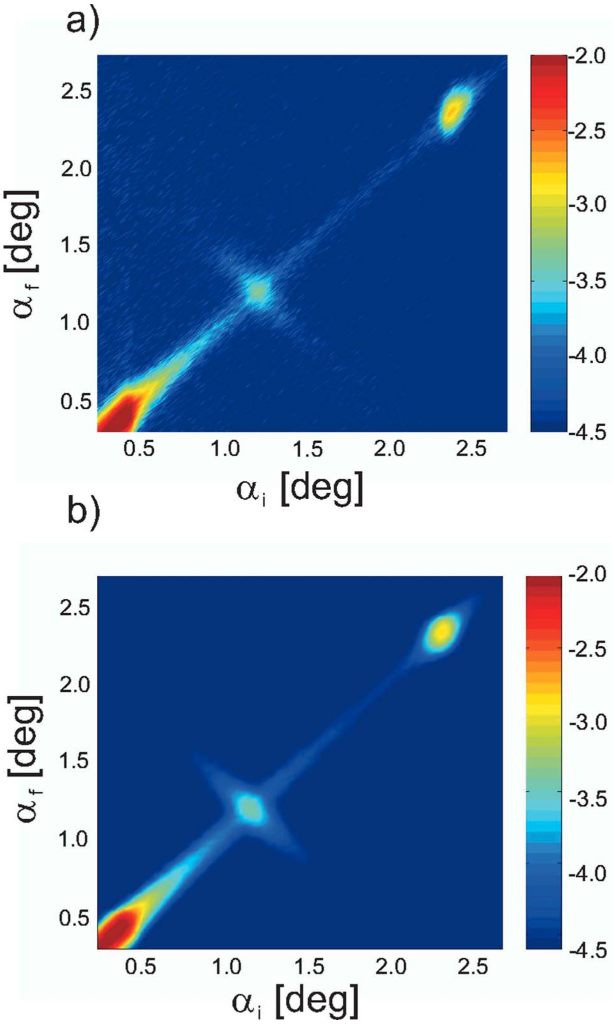

FIG. 11. (Color online) (a) 2D map of the neutron intensity scattered from the af coupled $[\mathrm{Co_2MnGe(3\ nm)/V(3\ nm)}]_{50}$ (#1) multilayer in zero applied field at 15 K. The Bragg sheet at the af peak is purely of magnetic ordering. The centered intensity is the first-order structural peak. (b) The simulation of the corresponding map within a super-iterative based version of the distorted wave Born approximation.

$-\alpha_f$ map of the scattering intensity of the $[\mathrm{Co_2MnGe(3\ nm)/V(3\ nm)}]_{50}$ (#1) multilayer in zero field measured at 15 K together with a simulation. The specular ridge with the first-order nuclear Bragg peak, as well as the Bragg sheet crossing the reflectivity ridge at the half-order Bragg peak position, can be observed. To achieve a good fit quality we simulated the map and directly compared the cut along the specular line and a vertical cut at the position of the af peak with the measured data. Simultaneously we provided spin-polarized simulations of the off-specular data using the same fitting parameters as for the unpolarized case and compared the reflectivity cuts through the maps with the measured polarized reflectivity scans (see simulation in Fig. 9). The maps were simulated within a super-iterative-based version of the distorted wave Born approximation (DWBA).[25,26] The underlying model has the following fit parameters: the lateral domain size ξ, the depth correlation factor n_0 giving the out-of-plane (af) correlation length, and the mean value $\langle \cos \varphi \rangle$ determining mean magnetization averaged over lateral domains in the coherence area, $\Delta\varphi$, giving deviations of domain magnetization vectors from the mean magnetization direction.

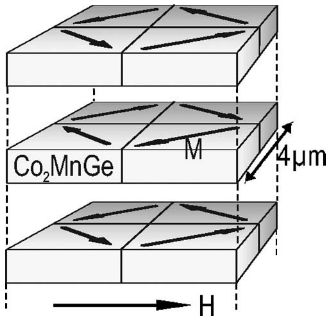

FIG. 12. Sketch of the microscopic picture for the antiferromagnetic state of the sample $[\mathrm{Co_2MnGe(3\ nm)/V(3\ nm)}]_{50}$ (#1) with four different types of domains. The arrow indicates the guiding field direction.

As the result from the numerical simulation we get the microscopic picture of small, completely coherent columnar domains with alternating angle $\Delta\varphi = 45°/225°$ and a lateral domain size of 2.1 μm. For the simulations the magnetic moments of the layers were set to 50% of the bulk value, in accordance with the magnetization measurements. Thus the sample breaks down into a Landau type of pattern[29] with four possible types of domains with perfect antiferromagnetic coupling (see Fig. 12).

For the multilayer with $t_V = 2$ nm the situation is quite different, although this sample also shows the transverse antiferromagnetic ordering and lateral domains. Similar to the previous case, essentially no splitting of the NSF cross sections at the structural first-order peak is apparent, i.e., no ferromagnetic contribution to the first-order peak in the magnetic ground state exists. But now, there is also no intensity in the SF channel apart from a very small peak at the position of the af peak, caused by not having 100% efficiency of the polarizing elements. The multilayer seems to be nearly perfectly af aligned with the sublattice magnetizations collinear with the guiding field. The collinear arrangement is, in fact, not very surprising, since it turned out that a growth-induced uniaxial magnetic anisotropy for the measurements in Fig. 9(a) is parallel to the direction of the external field. A relatively low guiding field for the neutron polarization does not cause a spin-flop transition into the state with the magnetization direction perpendicular to the field.[30]

In contrast to the previous case, Q_x scans through the af peak show a resolution-limited Gaussian line shape for the specularly reflected beam. The latter is superimposed onto an almost flat background of diffuse scattering (not shown here). This indicates the presence of antiferromagnetic ordering on a scale bigger than the neutron coherence length simultaneously with the magnetization fluctuations on a shorter length scale. Unfortunately neither of those scales can immediately be determined from the data: the specular peak width gives just a lower limit (60 μm) for the long-range af order, while af fluctuations contributing to diffuse scattering are too small in size to be deduced from the line

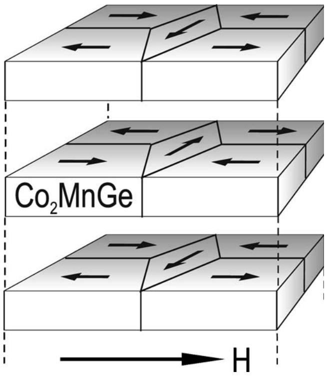

FIG. 13. Sketch of the microscopic picture for the antiferromagnetic state of the sample $[\mathrm{Co_2MnGe(3\ nm)/V(2\ nm)}]_{50}$ with two kinds of domains: large domains separated by 180° domain wall and "closure" domains. The arrow indicates the guiding field direction.

shape analysis of off-specular scattering, as the range of the lateral moment transfer is restricted.

On the other hand, the diffuse intensity contribution at the position of the specular reflection is small with respect to the Gaussian component. This justifies the fitting procedure of the reflectivity line in Fig. 9(a) described above and proves the values of the deduced physical parameters for this sample. The reduction of the sublayer magnetization values is due to the averaging of the layer magnetization over lateral domains within the coherence range. A domain configuration which can explain our observations for this sample is sketched in Fig. 13. Again, the data suggest that in each of the lateral and columnar-like domains the magnetization of the sublayers alters sign across the multilayer stack. However, now one can distinguish between two kinds of domains. The main set of relatively large domains separated by 180° domain wall mostly cause non-spin-flip specular reflection, as the domain magnetization is collinear with the guiding field for the neutron polarization. The size of those domains allows a few of them to be simultaneously illuminated coherently. Namely, this coherent averaging reduces the effective magnetic optical potential, while fluctuations around its mean value contribute in non-spin-flip off-specular scattering. The other set of so-called "closure" small domains[29] causes a diffuse background of spin-flip scattering. In the present experiments polarization analysis of diffuse scattering was not possible. Therefore the contribution of the closure domains to the off-specular scattering cannot be determined unambiguously. More detailed study of diffuse scattering is, however, not required to achieve our main goal: to learn about the remagnetization process in this system.

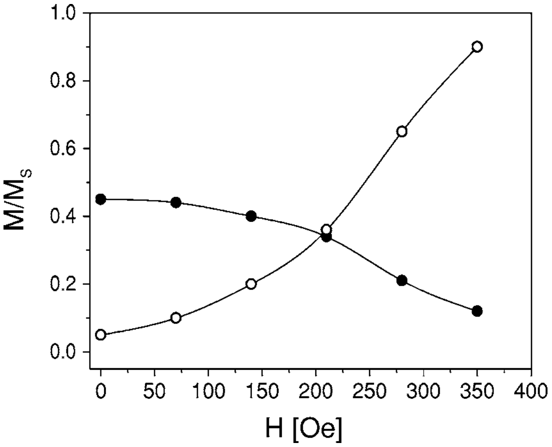

FIG. 14. Field dependence of the antiferromagnetic, $(m_1 - m_2)/2$ (filled circles), and ferromangnetic, $(m_1+m_2)/2$ (open circles), order parameters for the sample $[\mathrm{Co_2MnGe(3\ nm)/V(2\ nm)}]_{50}$ measured at 10 K.

Instead, it is sufficient to carry out corresponding fits for the specular reflectivity curves. The latter were measured on the $[\mathrm{Co_2MnGe(3\ nm)/V(2\ nm)}]_{50}$ multilayer at different fields at 10 K. To ensure a well-defined magnetic state, the sample has been saturated at room temperature and cooled down in zero field. The results of the fit are summarized in Fig. 14 where the field dependence of the antiferromagnetic, $(m_1 - m_2)/2$, and ferromangnetic, $(m_1+m_2)/2$, order parameters is depicted. With increasing field the af order parameter continuously decreases and is completely suppressed at $H = 350$ Oe. On the contrary, the ferromagnetic order parameter, almost vanishing in zero field, increases continuously, reaching the value expected for ferrromagnetic saturation at $H = 350$ Oe. Remembering that this sample has an antiferromagnetic configuration collinear with the applied field, one should expect some scattering intensity in the spin-flip channel, if the system would undergo a spin-flop transition and approach the saturation via rotation of the sublattice magnetization. Surprisingly, however, the remagnetization process is quite different. There is no resolvable spin-flip scattering over the entire magnetic field range (Fig. 15), indicating that the remagnetization takes place solely by domain wall movements for domains in the sublayer with the magnetization direction opposite to the applied field. From the upper panel in Fig. 15 it follows that the af order parameter continuously degrades as the intensity of the half-order af reflection decreases. Simultaneously the increasing ferromagnetic order parameter manifests itself in the splitting of the $(++)$ and $(--)$ channel intensities (lower panel in Fig. 15). At saturation the $(--)$ channel exhibits nearly zero intensity. This is

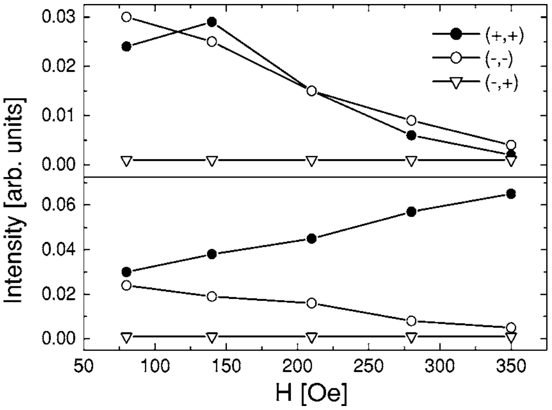

FIG. 15. Field dependence of the af peak intensity (upper panel) and first order structural peak (lower panel) for the spin flip $(-+)$ and non-spin flip $[(++)$ and $(--)]$ channels for the multilayer $[\mathrm{Co_2MnGe(3\ nm)/V(2\ nm)}]_{50}$ at 10 K.

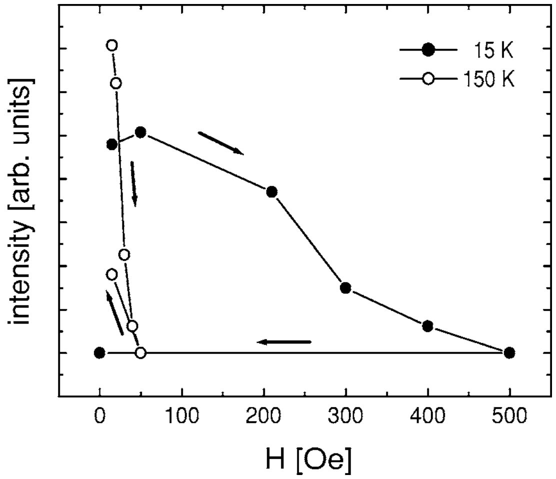

FIG. 16. Field dependence of the af peak intensity of the $[\mathrm{Co_2MnGe(3\ nm)/V(3\ nm)}]_{50}$ (#2) multilayer taken at $T=15$ K (solid dots) and $T=150$ K (open dots).

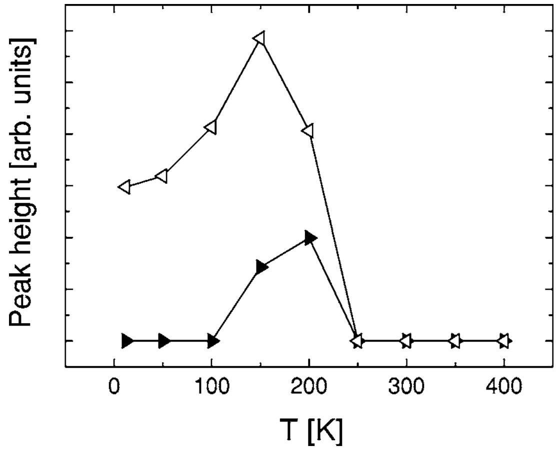

FIG. 17. Temperature dependence of the af peak intensity of the multilayer $[\mathrm{Co_2MnGe(3\ nm)/V(3\ nm)}]_{50}$ (#1) measured after field cooling (solid triangles) and zero field cooling (open triangles).

a special feature of several Heusler alloys, which has been used for the construction of neutron polarizers.[31]

Figure 16 shows the field dependence of the af peak intensity of the $[\mathrm{Co_2MnGe(3\ nm)/V(3\ nm)}]_{50}$ multilayer taken at 15 K and 150 K. At 15 K the af peak intensity is not restored after switching off the field, whereas at 150 K about 30% of the af peak intensity is restored. The af coupling is apparently very weak at 150 K; a field of about 50 Oe already destroys the af order. For antiferromagnetically coupled multilayers the effective coupling energy J can be estimated by the formula[32]

$$J = M_S t_{\mathrm{Heusler}} H_S/4, \tag{1}$$

where M_{S} is the saturation magnetization, t_{Heusler} is the thickness of a single $\mathrm{Co_2MnGe}$ layer, and H_{S} is the ferromagnetic saturation field. The values obtained by Eq. (1) are $J=6.8\times10^{-7}\ \mathrm{J/m^2}$ for the $[\mathrm{Co_2MnGe(3\ nm)/V(2\ nm)}]_{50}$ multilayer and $J=1.1\times10^{-7}\ \mathrm{J/m^2}$ for the sample $[\mathrm{Co_2MnGe(3\ nm)/V(3\ nm)}]_{50}$. Compared to typical values for, e.g., Co/Cu superlattices of the order of $10^{-4}\ \mathrm{J/m^2}$, the coupling strength in our samples is very weak.[33] The temperature dependence of the af peak intensity for the $[\mathrm{Co_2MnGe(3\ nm)/V(3\ nm)}]_{50}$ multilayer as measured after cooling in zero field and after cooling in a field of 1000 Oe and then switching off the field at the measuring temperature is displayed in Fig. 17. After zero-field cooling the af peak intensity develops below 250 K in a phase-transition-like fashion, reaches a maximum at about 150 K, and decreases slightly towards lower temperatures. After cooling in a field of 1000 Oe there is no detectable af peak intensity below 100 K, but, approaching the phase transition at $T_N=250$ K, the af order recovers after switching off the field. Close to the transition temperature the peak intensity coincides with that measured after zero-field cooling. Since the half-order peak intensity is proportional to the squared sublattice magnetization in an antiferromagnet, this behavior clearly reveals a reversible phase transition at 250 K. Remarkably this temperature is far below the ferromagnetic ordering temperature of a single $\mathrm{Co_2MnGe}$ film of comparable thickness, which is about 600 K.[34]

V. MAGNETIC PHASE DIAGRAM

The neutron scattering results of the previous section clearly prove that in the $[\mathrm{Co_2MnGe/V}]$ multilayers there is antiferromagnetic interlayer ordering in the thickness range $t_{\mathrm{V}}\leq 3$ nm. The Néel temperature derived from the peak in the susceptibility and the vanishing intensity of the half-order peak are combined in a magnetic phase diagram in Fig. 18. The Néel temperature decreases continuously with increasing thickness of the V layers. There is no indication of an oscillatory character of the magnetic coupling. We have confirmed for additional intermediate thicknesses by magnetization measurements that the interlayer ordering is always antiferromagnetic. Actually the magnetic state of the

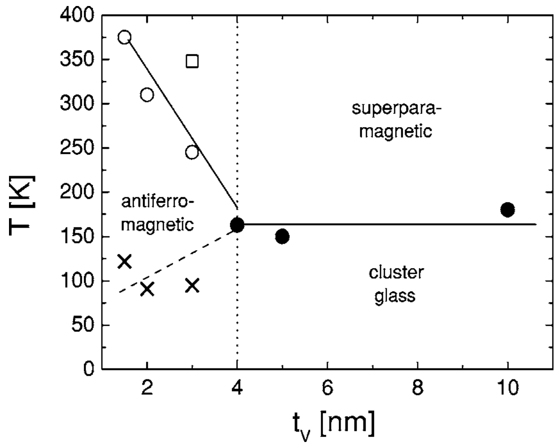

FIG. 18. Magnetic phase diagram for multilayers $[\mathrm{Co_2MnGe(3\ nm)/V}(t_V)]_{50}$ as a function of the V thickness t_V with the Néel temperature (open circles) and cluster glass temperature (filled circles). The open square designates T_N for the sample $[\mathrm{Co_2MnGe(3\ nm)/V(3\ nm)}]_{50}$ (#2), (see Table I). The crosses indicate the onset of a strong magnetic irreversibility.

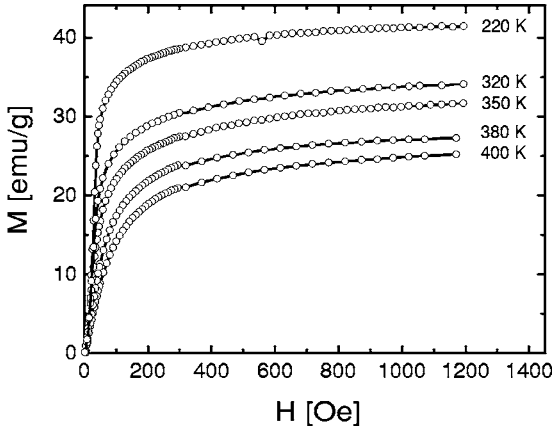

FIG. 19. Magnetization curves of the multilayer $[\mathrm{Co_2MnGe(3\ nm)/V(3\ nm)}]_{50}$ (#1) measured at different temperatures T given in the figure.

$[\mathrm{Co_2MnGe/V}]$ multilayers above the Néel temperature is not simply paramagnetic but exhibits superparamagnetic properties. In Fig. 19 the reversible magnetization of the $[\mathrm{Co_2MnGe(3\ nm)/V(3\ nm)}]_{50}$ multilayer for temperatures above T_{N} is depicted. The magnetization curves reveal typical superparamagnetic behavior with a linear $M(H)$ curve at low fields and saturation at higher fields. For non-interacting superparamagnetic clusters the magnetization should scale as[35]

$$M(H,T) = N_c\mu_c\mathcal{L}\left(\frac{\mu_c H}{k_b T}\right) \tag{2}$$

with the number of magnetic clusters N_c, the cluster magnetic moment μ_c, and the Langevin function $\mathcal{L}(x)$. Using the approximation $\mathcal{L}(x)\approx 1/3x$ valid for small x, the low field magnetization is given by

$$M(H,T) = \frac{N_c\mu_c^2 H}{3k_b T}. \tag{3}$$

Fitting formula (3) to the $M(H,T)$ curves in Fig. 19 we derive a cluster moment of $1.6\times 10^5\ \mu_B$ at 400 K. At 250 K, just above the Néel temperature, we get $\mu_c = 4\times 10^5\ \mu_B$. This magnetic moment corresponds to 7×10^5 or 2×10^6 $\mathrm{Co_2MnGe}$ formula units combining one cluster and gives an average dimension of $120\times 120\ \mathrm{nm}^2$ or $200\times 200\ \mathrm{nm}^2$, respectively, for the lateral cluster size. The superparamagnetic cluster type of behavior is similar for all multilayers of the present study. In Fig. 20 we compare the temperature development of the superparamagnetic cluster moments for the thickness $t_{\mathrm{V}}=3$ nm and $t_{\mathrm{V}}=4$ nm, where only the former compound orders antiferromagnetically. The temperature dependence of the cluster moment indicates that the clusters are not independent, but show interaction.[35] Thus the antiferromagnetic interlayer magnetic ordering in the $[\mathrm{Co_2MnGe/V}]$ multilayers develops from a superparamagnetic state and not from a conventional paramagnetic state. An interesting question concerns the magnetic order of the samples with $t_{\mathrm{V}} \geqslant 4$ nm which do not exhibit an antiferromagnetic interlayer order. Here one finds all ingredients of a cluster glass transition at a transition temperature T_{f}. Below T_{f} the coercive force strongly increases (Fig. 21), which can approximately be described by $H_c \propto H_0 e^{-\alpha T}$. The onset of strong irreversibility in the low field susceptibility occurs below the cluster glass transition temperature $T_{\mathrm{f}} \approx 150$ K.[36,37]

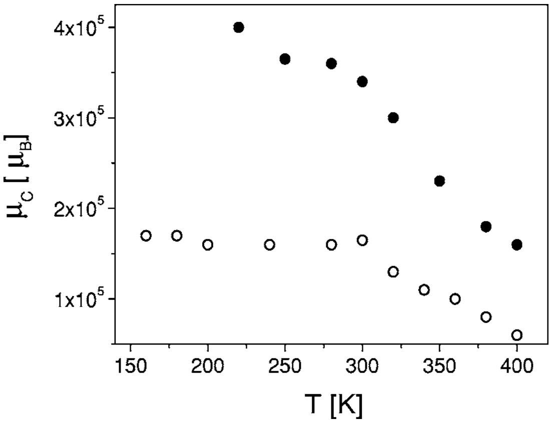

FIG. 20. Temperature dependence of the cluster magnetic moment μ_C for the $[\mathrm{Co_2MnGe(3\ nm)/V(3\ nm)}]_{50}$ (#1) multilayer (filled circles) and the $[\mathrm{Co_2MnGe(3\ nm)/V(4\ nm)}]_{50}$ multilayer (open circles).

We have included the cluster glass transition temperature T_f in the phase diagram of Fig. 18. It is essentially independent of the thickness t_{V}. The cluster glass transition continues below the antiferromagnetic phase transition line (see dashed line in Fig. 18) where it characterizes the onset of strong magnetic irreversibility below T_N. This line resembles the reentrance phase transition line which is found in conventional spin glass systems close to the critical concentration of long-range order.[24] This line is usually discussed in terms of the coexistence of both, the short- and the long-range order parameters, at low temperatures.

A. Discussion

We now discuss the microscopic origin leading to the peculiar magnetic phase diagram in Fig. 18. There are two

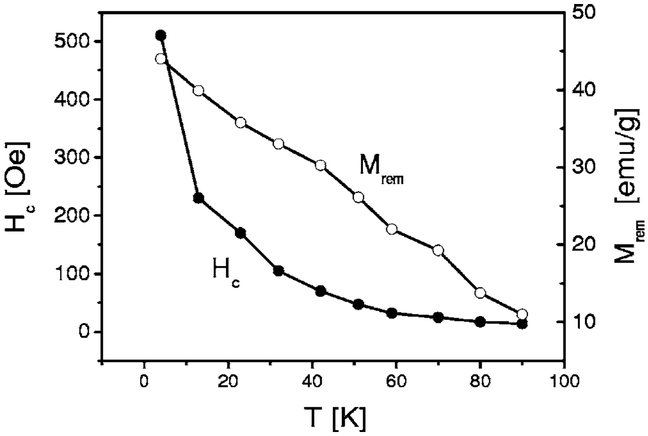

FIG. 21. Coercive field (solid circles) and remanent magnetization (open circles) versus temperature for the multilayer $[\mathrm{Co_2MnGe(3\ nm)/V(3\ nm)}]_{50}$ (#1).

essential ingredients one has to explain. The first is the origin of the cluster type magnetism, which is most obvious in the superparamagnetic behavior at high temperatures, and in the cluster glass transition at low temperatures. Second, the question concerning the magnetic interactions causing the formation of the antiferromagnetic interlayer ordering needs to be clarified.

The magnetic-cluster-type behavior is related to the crystalline microstructure of the single Co_2MnGe layers in the multilayer. We have shown in a previous investigation that a single 3 nm thick Co_2MnGe layer embedded between two V layers exhibits typical small particle ferromagnetism with a ferromagnetic hysteresis loop virtually identical for the magnetic field applied perpendicular and parallel to the film plane, although the surface of the magnetic film is atomically flat.[38] The reason for this cluster type of ferromagnetism is that the very small crystalline grains in the Co_2MnGe film are magnetically decoupled at the grain boundaries which are chemically disordered and weakly ferromagnetic.[38] A superparamagnetic high-temperature state is the natural consequence of small particle magnetism, if the interactions between the clusters are weak and the magnetic anisotropy is small. In contrast, in a single Co_2MnGe thin film grown on a V seed layer we did not observe superparamagnetism in the temperature range up to the maximum experimental temperature of 400 K. In the $[Co_2MnGe/V]$ multilayers with the same thickness of the magnetic layers, however, superparamagnetic behavior already exists at room temperature, probably due to a slightly different microstructure and a larger topological roughness of the Co_2MnGe layers. Thus alloying and roughening at the interfaces and atomic disorder at the grain boundaries cause the Co_2MnGe layers in the multilayers to break up into weakly coupled magnetic clusters. The mean grain size of the crystallites in the multilayers as determined from the off-specular x-ray reflectivity is about 20 nm. The average lateral magnetic cluster size we derived from the superparamagnetic moment just above T_{N} is of the order of 200 nm, i.e., one magnetic cluster is combined of many crystalline grains. In the antiferromagnetically ordered phase we determined an average lateral size for the magnetic domains of several μm. Thus, in the antiferromagnetically ordered state many magnetic clusters within one Co_2MnGe layer belong to one magnetic domain.

Concerning the magnetic interactions responsible for the antiferromagnetic interlayer magnetic ordering, we can exclude interlayer exchange coupling. Nonferromagnetic interfaces and thickness fluctuations seem to weaken the IEC coupling drastically. We are thus led to the conclusion that the dipolar interactions between the planes cause the antiferromagnetic interlayer ordering. This would explain the absence of an oscillatory character of the interlayer coupling and the weak antiferromagnetic coupling field. Actually dipolar stray fields protruding at the grain boundaries are a natural consequence of the internal granular structure of the Co_2MnGe films. In Fig. 22 we have drawn schematically how interlayer dipolar interactions may arrange the antiferromagnetic interlayer order in the $[Co_2MnGe/V]$ multilayer system.

The importance of interlayer dipolar interactions in multilayer systems is well established in the literature. Theoretical model calculations show that the dipolar coupling in multilayers can be ferromagnetic or antiferromagnetic, depending on the interface topology.[39–42] In a system with corrugated interfaces the so-called "orange peel" coupling[43] may give rise to a ferromagnetic interlayer coupling. For the case of uncorrelated roughness, antiferromagnetic coupling is more probable.[40] Experimentally an antiferromagnetic interlayer ordering induced by dipolar interactions has been observed in [Co/Cu] multilayers with 6 nm thick Cu layers.[42] In multilayer systems [Nb/Fe] and [FeNi/Ag], af interlayer order due to dipolar interactions has also been discussed.[44,45] However, at variance to the system studied here, none of these multilayers exhibits a reversible af phase transition and a superparamagnetic state above the Néel temperature.

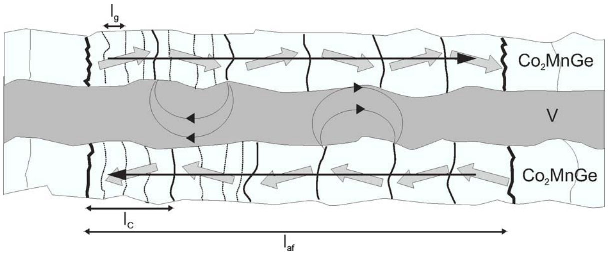

FIG. 22. (Color online) Schematic picture of the interlayer order in the $[Co_2MnGe(3\ \mathrm{nm})/V(t_V)]_N$ multilayers. The size of the crystallites is about $l_g=20$ nm, the average magnetic cluster size is of the order $l_c=200$ nm, and the size for the magnetic domains l_{af} is of several μm. The arrows indicate the direction of the local magnetization.

VI. SUMMARY AND CONCLUSION

We have studied the structural and magnetic properties of a series of sputter-deposited $[Co_2MnGe/V]$ multilayers, using x-ray and neutron reflectivity techniques and magnetization measurements. X-ray reflectivity confirms the growth of a multilayer structure with smooth interfaces. Off-specular x-ray scattering reveals a mainly uncorrelated roughness with an in-plane correlation length $L_h=20$ nm corresponding to the average crystallite size. Bragg scans give an out-of-plane coherence length $L_h=13$ nm. PNR and magnetization measurements indicate a magnetic phase transition at a Néel temperature T_N with simultaneous ferromagnetic order in the Co_2MnGe layers and antiferromagnetic order between the layers. Above T_N the magnetic layers are superparamagnetic. Antiferromagnetic order with a weak coupling strength and without any indication of an oscillatory character is observed for the thickness range $t_{\mathrm{V}} \leqslant 3$ nm.

We attribute the observed antiferromagnetic interlayer ordering to magnetic stray fields arising from the granular Heusler layers. The interlayer dipolar interactions cause a reversible magnetic phase transition of the magnetic clusters with antiferromagnetic order between the layers at a well-defined Néel temperature for $t_{\mathrm{V}} \leqslant 3$ nm. If the V layer thickness is larger, the dipolar forces are too weak to arrange antiferromagnetic long range order and the system undergoes a cluster glass transition at temperatures of about 150 K.

ACKNOWLEDGMENTS

The authors thank the DFG for financial support of this work within the SFB 491 and S. Erdt-Böhm for sample preparation. The neutron work carried out with the ADAM reflectometer at the Institute Laue Langevin is supported by BMBF under Contract No. O3ZAE8BO.

---

*Electronic address: andre.bergmann@ruhr-uni-bochum.de

[†] Gerhad Mercator Guest Professor under appointment with DFG.

[1] G. Prinz, Science **282**, 1660 (1998).

[2] D. Awschalom and J. Kikkawa, Phys. Today **52**, 33 (1999).

[3] J. F. Gregg, I. Petej, E. Jouguelet, and C. Dennis, J. Phys. D **35**, R121 (2002).

[4] R. A. de Groot, F. M. Mueller, P. van Engen, and K. H. J. Buschow, Phys. Rev. Lett. **50**, 2024 (1983).

[5] S. Ishida, T. Masaki, S. Fujii, and S. Asano, Physica B **245**, 1 (1998).

[6] C. Felser, B. Heitkamp, F. Kronast, D. Schmitz, S. Cramm, H. A. Dürr, H.-J. Elmers, G. H. Fecher, S. Wurmehl, T. Block, D. Valdaitsev, S. A. Nepijko, A. Gloskovskii, G. Jakob, G. Schönhense, and W. Eberhardt, J. Phys.: Condens. Matter **15**, 7019 (2003).

[7] J. S. Moodera, L. R. Kinder, T. M. Wong, and R. Meservey, Phys. Rev. Lett. **74**, 3273 (1995).

[8] B. Dieny, J. Magn. Magn. Mater. **136**, 335 (1994).

[9] C. Tanaka, J. Novak, and J. S. Moodera, J. Appl. Phys. **81**, 5515 (1997).

[10] J. Schmalhorst, S. Kämmerer, M. Sacher, G. Reiss, A. Hütten, and A. Scholl, Phys. Rev. B **70**, 024426 (2004).

[11] K. Inomata, S. Okamura, R. Goto, and N. Tezuka, Jpn. J. Appl. Phys., Part 2 **42**, L419 (2003).

[12] I. Galanakis, J. Phys.: Condens. Matter **14**, 6329 (2002).

[13] U. Geiersbach, A. Bergmann, and K. Westerholt, Thin Solid Films **425**, 226 (2003).

[14] P. Bruno, Phys. Rev. B **52**, 411 (1995).

[15] A. Bergmann, J. Grabis, V. Leiner, M. Wolf, H. Zabel, and K. Westerholt, Superlattices Microstruct. **34**, 137 (2003).

[16] H. Zabel, Appl. Phys. A: Solids Surf. **58**, 159 (1994).

[17] D. E. Savage, J. Kleiner, N. Schimke, Y.-H. Phang, T. Jankowski, J. Jacobs, R. Kariotis, and M. G. Lagally, J. Appl. Phys. **69**, 1411 (1991).

[18] S. K. Sinha, E. B. Sirota, S. Garoff, and H. B. Stanley, Phys. Rev. B **38**, 2297 (1988).

[19] A. Scheyer, R. Siebrecht, U. English, U. Pietsch, and H. Zabel, Physica B **267–268**, 355 (1999).

[20] H. Dosch, K. Alusta, A. Lied, W. Drexel, and J. Peisl, Rev. Sci. Instrum. **63**, 5533 (1992).

[21] L. G. Parratt, Phys. Rev. **95**, 359 (1954).

[22] Z. H. Mingh, A. Krol, Y. L. Soo, Y. H. Kao, J. S. Park, and K. L. Wang, Phys. Rev. B **47**, 16373 (1993).

[23] B. E. Warren, *X-ray Diffraction* (Dover Publications, Inc., New York, 1990).

[24] K. Binder and A. Young, Rev. Mod. Phys. **58**, 801 (1986).

[25] B. Toperverg, in *Polarized Neutron Scattering*, edited by T. Brückel and W. Schweika (Schriften des Forschungszentrum Jülich, 2002), Matter and Materials, Vol. 12.

[26] U. R. E. Kentzinger and B. Toperverg, Physica B **335**, 82 (2003).

[27] B. Toperverg, A. Rühm, W. Donner, and H. Dosch, Physica B **267–268**, 198 (1999).

[28] A. Rühm, B. P. Toperverg, and H. Dosch, Phys. Rev. B **60**, 16073 (1999).

[29] A. Hubert and R. Schäfer, *Magnetic Domains. The Analysis of Magnetic Microstructures* (Springer, Berlin, 1998).

[30] V. Lauter-Pasyuk, H. J. Lauter, B. P. Toperverg, L. Romashev, and V. Ustinov, Phys. Rev. Lett. **89**, 167203 (2002).

[31] A. Delapalme, J. Schweizer, G. Couderchon, and R. P. de la Bathie, Nucl. Instrum. Methods Phys. Res. A **95**, 589 (1994).

[32] A. Bartélémy, A. Fert, M. Baibich, S. Hadjoudj, F. Petroff, P. Etienne, R. Cabanel, S. Lequien, F. N. V. Dau, and G. Creuzet, J. Appl. Phys. **67**, 5908 (1990).

[33] D. Bürgler, P. Grünberg, S. Demokritov, and M. Johnson, in *Handbook of Magnetic Materials, Vol. 13*, edited by K. Buschow (Elsevier, Amsterdam, 2002).

[34] U. Geiersbach, A. Bergmann, and K. Westerholt, J. Magn. Magn. Mater. **240**, 546 (2002).

[35] B. Culity, *Introduction to Magnetic Materials* (Addison-Wesley, London, 1972).

[36] K. Fischer, Phys. Status Solidi B **120**, 13 (1985).

[37] J. A. Mydosh, *Spin Glasses: An Experimental Introduction* (Taylor & Francis, London, 1993).

[38] K. Westerholt, A. Bergmann, J. Grabis, A. Nefedov, and H. Zabel, in *Half-metallic Alloys-Fundamentals and Applications*, Lecture Notes in Physics, edited by P. Dederichs and J. Galanakis (Springer, New York, 2005).

[39] D. Altbir, M. Kiwi, R. Ramírez, and I. K. Schuller, J. Magn. Magn. Mater. **149**, L246 (1995).

[40] J. P. Hill and D. F. McMorrow, Acta Crystallogr., Sect. A: Found. Crystallogr. **52**, 236 (1996).

[41] J. C. Slonczewski, J. Magn. Magn. Mater. **150**, 13 (1995).

[42] J. A. Borchers, P. M. Gehring, R. W. Erwin, J. F. Ankner, C. F. Majkrzak, T. L. Hylton, K. R. Coffey, M. A. Parker, and J. K. Howard, Phys. Rev. B **54**, 9870 (1996).

[43] L. Néel, C. R. Hebd. Seances Acad. Sci. **255**, 1676 (1962).

[44] J. A. Borchers, J. A. Dura, J. Unguris, D. Tulchinsky, M. H. Kelley, C. F. Majkrzak, S. Y. Hsu, R. Loloee, W. P. Pratt, and J. Bass, Phys. Rev. Lett. **82**, 2796 (1999).

[45] C. Rehm, D. Nagengast, F. Klose, H. Maletta, and A. Weidinger, Europhys. Lett. **38**, 61 (1997).